JACS
JOURNAL OF THE AMERICAN CHEMICAL SOCIETY

Article

pubs.acs.org/JACS

Amine Oxidation Mediated by Lysine-Specific Demethylase 1: Quantum Mechanics/Molecular Mechanics Insights into Mechanism and Role of Lysine 661

Bora Karasulu, Mahendra Patil,[†] and Walter Thiel*

Max-Planck-Institut für Kohlenforschung, Kaiser-Wilhelm-Platz 1, 45470 Mülheim, Germany

Supporting Information

ABSTRACT: We report classical molecular dynamics (MD) simulations and combined quantum mechanics/molecular mechanics (QM/MM) calculations to elucidate the catalytic mechanism of the rate-determining amine oxidation step in the lysine-specific demethylase 1 (LSD1)-catalyzed demethylation of the histone tail lysine (H3K4), with flavin adenine dinucleotide (FAD) acting as cofactor. The oxidation of substrate lysine (sLys) involves the cleavage of an α-CH bond accompanied by the transfer of a hydride ion equivalent to FAD, leading to an imine intermediate. This hydride transfer pathway is shown to be clearly favored for sLys oxidation over other proposed mechanisms, including the radical (or single-electron transfer) route as well as carbanion and polar-nucleophilic mechanisms. MD simulations on six NVT ensembles (covering different protonation states of sLys and K661 as well as the K661M mutant) identify two possible orientations of the reacting sLys and FAD subunits (called "downward" and "upward"). Calculations at the QM(B3LYP-D/6-31G*)/CHARMM22 level provide molecular-level insights into the mechanism, helping to understand how LSD1 achieves the activation of the rather inert methyl-CH bond in a metal-free environment. Factors such as proper alignment of sLys (downward orientation), transition-state stabilization (due to the protein environment and favorable orbital interactions), and product stabilization via adduct formation are found to be crucial for facilitating the oxidative α-CH bond cleavage. The current study also sheds light on the role of important active-site residues (Y761, K661, and W695) and of the conserved water-bridge motif. The steric influence of Y761 helps to position the reaction partners properly, K661 is predicted to get deprotonated prior to substrate binding and to act as an active-site base that accepts a proton from sLys to enable the subsequent amine oxidation, and the water bridge that is stabilized by K661 and W695 mediates this proton transfer.

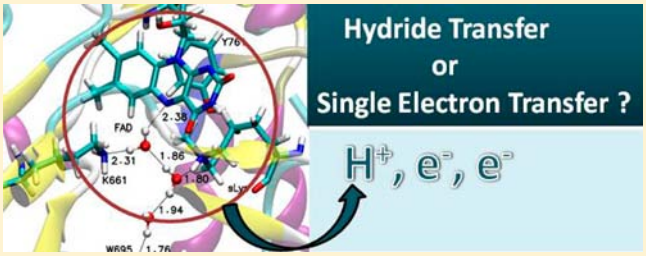

INTRODUCTION

Chromatins, the basic structural units of genetic material, are used for DNA packaging in eukaryotes. They are mainly composed of aggregates of the nucleosome, an octamer of four different histones.[1] Eukaryotic DNA is wrapped around the histone cores, forming a bead-like structure. In order to access the genetic information, chromatin is partially unwound during gene expression, transcription, DNA repair, replication, and related processes.[2] Histone proteins regulate gene transcription by altering the chromatin structure via post-translational modifications performed on their tails.[3] These modifications are carried out at target sites, which include the N-terminus of a specific lysine or arginine residue at a specific histone tail, each site being related to important cell regulatory processes.[4] They essentially involve covalent addition/removal of a chemical group to/from the site of interest. Among these post-translational modifications, only methylation had long been thought to be irreversible, as the half-life of methylated histone tails is longer than that of the wild-type (non-methylated) histones.[5] The possibility of demethylation was raised by observations on rat kidney in 1973[6] and confirmed by the discovery in 2004 of the first human histone demethylase, lysine-specific demethylase 1 (LSD1),[7] showing that the methylation of the histone tail is dynamically controlled by the reverse demethylation process.

LSD1 is a monoamine oxidase (MAO) that depends on flavin adenine dinucleotide (FAD). It specifically catalyzes the demethylation of methyl and dimethyl (not trimethyl) lysine residues at the fourth position of the histone H3 protein tails (H3K4).[8] LSD1 shows a slight preference for dimethyl lysine over methyl lysine, with turnover rates of 8.10 ± 0.20 and 3.40 ± 0.10 min^{-1}, respectively.[8] Judging from the very low turnover rates, 2−5 orders of magnitude smaller than those of other types of flavoprotein amine oxidases, LSD1 has apparently evolved for substrate specificity rather than catalyst efficiency.[9] The high substrate specificity has been linked to the need for direct interaction of the active site of LSD1 with at least 21 neighboring residues on the tail of H3 protein and the need to orient the methylated substrate lysine in front of the *re*-face of the cofactor FAD to enable proper enzymatic activity.[10,11] Therefore, LSD1 possesses a significantly larger binding pocket

Received: April 10, 2013
Published: August 15, 2013

dx.doi.org/10.1021/ja403582u | J. Am. Chem. Soc. 2013, 135, 13400−13413

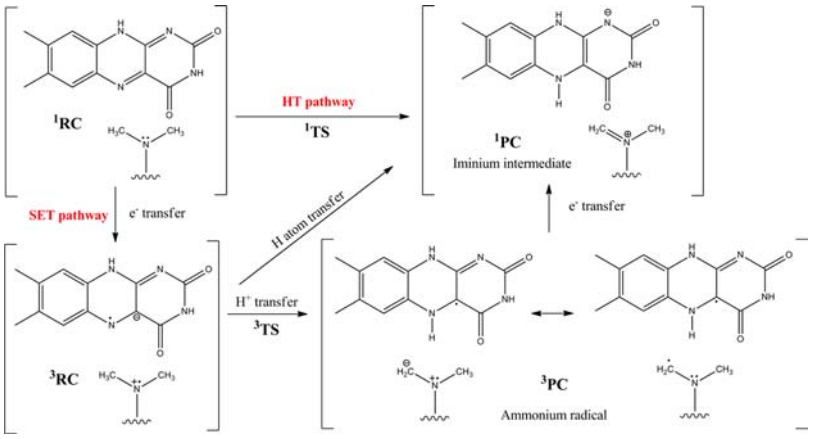

Figure 1. Direct hydride transfer (HT) and radical (SET) pathways proposed for the amine-oxidation step of lysine demethylation catalyzed by LSD1. Abbreviations: RC/PC, reactant/product complex; TS, transition state.

than other amine oxidases. LSD1 is a component of a multiprotein repressor complex, which is controlled by the repressor element 1-silencing transcription (REST). LSD1 binds a corepressor (CoREST) via its TOWER domain.[4] Its interaction with CoREST not only enables the demethylation of the histone H3K4 substrate but also stabilizes LSD1 and increases the enzymatic activity 2-fold.[1] LSD1 can also operate on nonhistone substrates, p53,[12] DNMT,[13] and MYPT1.[14] This allows LSD1 to regulate many vital cell-regulatory processes.[3] It has been shown that abnormal activity of LSD1 is related to many diseases, especially to some cancer types, heart diseases, diabetes, and neurodegenerative disorders, such as Parkinson's disease and Alzheimer's disease.[15] Therefore, the discovery of potential inhibitor molecules that can regulate any abnormal demethylation/methylation balance in LSD1 is of current research interest.[16] From a drug discovery perspective, a molecular-level understanding of the mechanism of the LSD1-catalyzed demethylation process is essential.

LSD1 shows significant sequence identity with other types of amine oxidases, especially with regard to the domain that hosts the active-site cavity. The active site of LSD1 and of other flavoprotein amine oxidases is normally located close to the isoalloxazine moiety of the flavin.[1] Some structural motifs[1,17] are well conserved across flavin-dependent amine oxidases. Most importantly, a conserved lysine residue (K661 in LSD1) forms a hydrogen-bond network to the flavin via a conserved crystal water molecule juxtaposed to the reduction site of the flavin. This water-bridge motif is commonly considered to play an important role in enzymatic activity, which is supported by mutagenesis experiments that show a loss of LSD1 activity upon K661A mutation.[18] Mutation of the corresponding lysine to methionine in maize PAO (K300M) and mammalian PAO (K315M) leads to 1400-fold[19] and 1.8-fold[20] decreases in enzymatic activity, respectively. Based on these experimental findings, different roles for the conserved lysine have been proposed in different amine oxidases. These include participation in catalysis, steric positioning of the flavin ring,[20] and acting as an active-site base by accepting a proton from protonated lysine substrate.[9,19−21] The water-bridge motif has also been considered as the site of oxygen activation during the non-enzymatic oxidative half-reaction, because of the loss of enzymatic turnover and oxygen reactivity upon mutation of K259 in *N*-methyltryptophan oxidase (MTOX).[22]

Another important conserved motif in the active site of different amine oxidases is the aromatic cage, which consists of a pair of aromatic residues shielding the active site from the influx of external solvent molecules, by contributing to its hydrophobicity.[17] In LSD1, one of the two aromatic residues is replaced by threonine (Thr810), while one conserved tyrosine (Tyr761) is still present.[1] As in other amine oxidases, the conserved tyrosine in LSD1 (Tyr761) is located[10,11] next to the substrate binding site on the *re*-face of flavin in the plane orthogonal to the flavin ring. The close proximity of the conserved tyrosine residue to the substrate has been interpreted in terms of a steric role of this residue in aligning the substrate in front of the isoalloxazine ring, through H-bonding and π-cation interactions.[1] In addition, a mutation study on the sandwich-like Tyr-Tyr aromatic cage in human MAO-B[23] suggested that the cage environment enhances the nucleophilicity of the substrate amine moiety via repulsive interactions. Apart from structural aspects, the conserved tyrosine was reported to serve as the initial electron acceptor in MAO-A, through detection of the tyrosyl radical by EPR and ENDOR spectroscopy.[24] The observation of rapid redox equilibrium between the tyrosyl radical and the flavin in MAO-A is in accord with the fact that the tyrosine is covalently bound to the flavin through a cysteine. In contrast, FAD is non-covalently attached to LSD1, which may impede the capacity of Tyr761 in LSD1 to act as the initial electron acceptor. In summary, although the steric influence of the conserved tyrosine appears to be more pronounced than its catalytic relevance, there is still a clear need to determine the precise role of Tyr761 in LSD1.

The LSD1-catalyzed demethylation process involves removal of one methyl group (or of two such groups in two consecutive steps) from the N-terminal of the amine substrate (methylated histone H3K4) via a redox process. Shi et al.[7] proposed a three-step catalytic mechanism for histone demethylation. In the first step, the α-CH bond of the methyl group is cleaved, and the amine is oxidized via transfer of a hydride equivalent from the substrate to FAD. Primary deuterium isotope studies indicate that the breaking of the chemically inert α-CH bond is the rate-limiting step.[9] Amine oxidation is accompanied by two-electron reduction of FAD, which is then (in an oxidative half-reaction) re-oxidized by molecular oxygen with formation of a hydrogen peroxide molecule. This re-oxidation of FAD is a complementary process with high rates[8] that prepares FAD for the subsequent demethylation. In the remaining two steps of the

dx.doi.org/10.1021/ja403582u | J. Am. Chem. Soc. 2013, 135, 13400−13413

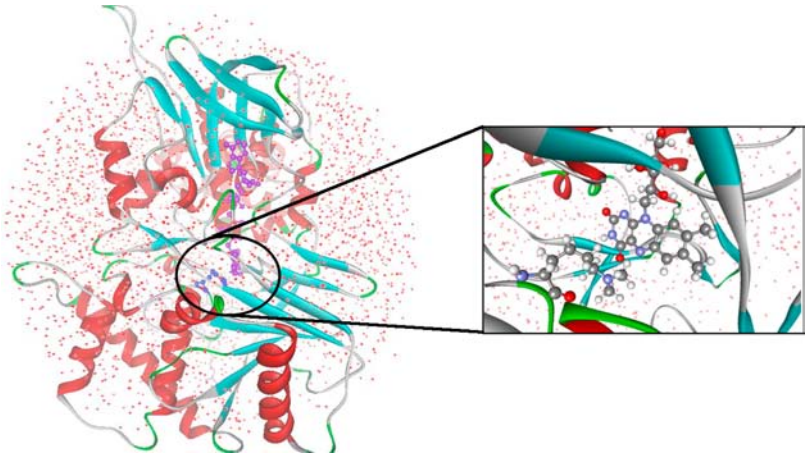

Figure 2. Representative snapshot of the simulation system: FAD and substrate H3K4 (sLys) are shown in ball-and-stick representation in blue and purple, respectively. In the enlarged active site view, the atoms are colored according to atom type (gray, carbon; white, hydrogen; blue, nitrogen; red, oxygen). The simulation system is solvated in a water droplet with radius of 35 Å.

demethylation process, the iminium intermediate is hydrolyzed and the resulting carbinol amine spontaneously rearranges to yield formaldehyde and the demethylated amine. These products have been identified by various experimental methods.[4] The proposed mechanism is supported by the binding mode of the substrate in the crystal structure of LSD1 in the presence of an inhibitor peptide[10] as well as by other experimental findings.[8] Consistent with the lack of a lone pair at the amino group in trimethyl lysines that is required in the proposed amine oxidation mechanism, LSD1 does not act on trimethyl lysines even though its spacious active site can accommodate trimethyl substrate binding.[25]

The rate-limiting first step of amine oxidation involves the transfer of a hydride equivalent from the amine substrate to FAD. The possibility of transferring two electrons and a proton in different order gives rise to several possible mechanisms, namely a direct hydride transfer (HT), a radical mechanism via single-electron transfer (SET),[26−28] and an adduct-forming mechanism.[29] The first two of these mechanisms are depicted in Figure 1 for the case of histone dimethyl lysine demethylation. Obviously, the simplest mechanism is the direct concerted transfer of the two electrons and a proton as a hydride anion from the α-carbon atom of the substrate to FAD. In the radical and adduct-forming mechanisms, there are intermediate species.

There are many studies that favor different mechanisms for different amine oxidases (see refs 1, 3, 17, 30−32 for comprehensive reviews). ^{15}N kinetic isotope effect (KIE) computations on MTOX[33] did not provide clear support to either the HT or SET mechanism. Cyclopropyl inhibitor studies on LSD1 were interpreted as being indicative of a SET mechanism,[34] but this view was challenged[9] on the grounds that some other flavoprotein oxidases, for which HT is considered the most likely mechanism, are also inactivated by cyclopropyl inhibitors.[35,36] The absence of any conceivable intermediate (i.e., a flavin or amine radical species) in kinetic, EPR, and ENDOR studies on LSD1[9,37] was taken as evidence in favor of the HT mechanism. The failure to find any intermediates by EPR or ENDOR spectroscopy was considered to be inconclusive by others,[27,33] however, on the basis of the following scenario: the initial SET process could be reversible (but not rate-limiting), with the back-transfer being much faster; this could lead to a very low concentration of the short-lived radical intermediates, which might not be visible in the EPR and ENDOR spectra.

These conflicting experimental findings on the LSD1 catalytic mechanism call for a theoretical study to monitor molecular-level details that are not directly observable experimentally. Here we report the results from molecular dynamics (MD) simulations as well as quantum mechanical (QM) and QM/molecular mechanical (QM/MM) calculations on the amine oxidation step of histone lysine demethylation. The objective is to assign the catalytic mechanism and to gain detailed molecular-level insight into the role of the active-site LSD1 residues (Lys661, Tyr761, and W695) and of the conserved water-bridge motif in the amine oxidation step.

Among the published computational studies on amine oxidases, only a few cover some aspects within the scope of the current work. A QM-only investigation on MTOX-mediated amine oxidation[33] addressed a simple model system consisting of a truncated isoalloxazine moiety of the flavin and dimethylamine $NH(CH_3)_2$ as the substrate. The computed DFT(B3LYP) energies were found to favor the direct hydride mechanism over the radical-SET mechanism for MTOX.[33] The first QM-only study on LSD1 demethylation was performed by Karasulu et al.[38] using semiempirical (PM3) and DFT (B3LYP) methods. However, the results were only preliminary and limited in scope. More recently, Kong et al.[39] reported classical MD and QM/MM (ONIOM) calculations on the mechanism of the LSD1-catalyzed amine oxidation, which support the HT mechanism. Their QM/MM study focused on the HT pathway and did not provide detailed information on other mechanisms. Moreover, they considered only one particular protonation state of sLys and the conserved K661 residue, and also only one representative snapshot of the system.[39] In the present study, we perform a more extensive sampling of the system by preparing six different NVT ensembles through 20 ns MD runs and by considering different possible protonation states and also mutation of the crucial K661 residue. This allows us to characterize two distinct orientations of sLys with respect to the isoalloxazine ring of FAD and to come up with a comprehensive mechanistic scenario of the events following substrate binding. Furthermore, the roles of important active-site LSD1 residues (K661, Y761, and W695) and of the conserved water-bridge motif are investigated in detail.

dx.doi.org/10.1021/ja403582u | J. Am. Chem. Soc. 2013, 135, 13400−13413

METHODS AND COMPUTATIONAL DETAILS

The simulations reported here are based on the crystal structure of LSD1 (PDB code 2V1D[10]) in complex with CoREST, the co-repressor that enables LSD1 to bind nucleosomal substrates and increases its activity, and with FAD, the cofactor that is non-covalently bound to LSD1 and acts as an oxidative agent in the demethylation process. The setup of the simulation system consisting of ca. 18 000 atoms (see Figure 2) is described in detail in the Supporting Information. Six different NVT ensembles were generated from six separate 20 ns MD simulation runs. Each of these six NVT ensembles corresponds to a different protonation state of K661 or the substrate dimethyl-K4, or involves K661M mutation. The classical MD simulations were performed with CHARMM[40] using a time step of 1 fs, and the atoms were coupled to a thermal bath at constant temperature (300 K). Spherical boundary conditions were imposed using the miscellaneous mean-field potential[40] to prevent the evaporation of solvent molecules. All bonds to hydrogen atoms were constrained by the SHAKE algorithm.[41] The duration (20 ns) of the productive MD simulation runs was sufficient to provide good starting points for the subsequent QM/MM calculations.

QM-only calculations were carried out using density functional theory (DFT) and the Gaussian09 program suite.[42] For this purpose, the full system was truncated to a model system that consisted of sLys, the isoalloxazine ring of FAD, and two active-site water molecules. Four different functionals (B3LYP,[43] M06-2X,[44] LC-ωPBE,[45] and mPW1K[46]) were utilized with the 6-31G* basis set in the gas-phase optimizations and the following vibrational analysis. No constraints were applied in the optimizations. Intrinsic reaction coordinate calculations were used for locating the reactant and product complexes (RC and PC) starting from the transition state (TS) connecting them.

Hybrid QM/MM studies of the full simulation system were performed with the ChemShell program suite.[47] The QM part of the system was computed at the DFT level (B3LYP/6-31G*[43]) using the TURBOMOLE 6.3 software;[48] Grimme-type dispersion corrections[49] were included in all single-point calculations and geometry optimizations. The ground-state singlet and the lowest triplet states were described using restricted and unrestricted Kohn–Sham (RKS and UKS) treatments, respectively. In addition, UKS calculations were performed for all putative open-shell singlet species to check whether they may yield an open-shell (radical-type) configuration with energy lower than that of the closed-shell configuration. The MM calculations were handled by the DL_POLY code[50] implemented in ChemShell using the CHARMM22 force-field parameters specified in the Supporting Information. The QM/MM treatment employed an electrostatic embedding in combination with the charge-shift scheme[51] and the atoms at the QM/MM boundary were treated by the link-atom approach.[47]

In the QM/MM calculations, the QM region consisted of FAD, K661, sLys, and three active-site water molecules (i.e., a total of 72–73 atoms, depending on the protonation state of K661). The included residues were truncated at appropriate sp^3-hybridized carbon atoms. To be specific, FAD was represented by the isoalloxazine ring, with a cut at the C1′–N10 bond (thus excluding the side chain), whereas the lysines were truncated at their C_β–C_γ bond (thus excluding their backbone parts). QM/MM geometry optimizations were carried out with the hybrid delocalized internal coordinates optimizer[52] implemented in ChemShell. Starting geometries for optimizations were taken from several snapshots of the canonical MD ensembles, and only residues within 15 Å of FAD were optimized in order to reduce the computational burden and also to retain the overall protein structure in the absence of CoREST. During the TS optimizations, the spatial positions of the atoms placed in the core region (i.e., those directly involved in the reaction) were optimized using the P-RFO algorithm, whereas the remaining non-frozen nuclei were treated by the L-BFGS algorithm. The optimized structures were subjected to numerical force constant calculations in ChemShell to determine the vibrational modes and to characterize the optimized stationary points (one negative eigenvalue of the corresponding Hessian matrix for TS, none for minima). Gibbs free energies (ΔG) and other thermodynamic properties were evaluated using the standard rigid-rotor harmonic oscillator approximation. Theoretical reaction rates were obtained from the relevant Gibbs free energy barrier $\Delta G^{\ddagger}$ (the free energy of activation) in the usual manner. Natural bond order analyses were performed using Gaussian09 to evaluate the Wiberg bond orders (with MM point charges included).

RESULTS

Changes in the Active Site upon Substrate Binding.

Compared with other flavin-dependent amine oxidases, the active site of LSD1 is rather wide and spacious.[11] It has four major invaginations with distinct chemical properties for the specific binding of side chains on the substrate H3 tail. The first pocket contains the isoalloxazine ring of the FAD cofactor forming the main catalytic hydrophobic chamber of LSD1, while the other three are required for accommodating the histone tail adjacent to the substrate lysine (sLys).[25] In the first pocket, the isoalloxazine moiety is surrounded by the residues Arg310, Arg316, Val317, Gly330, Ala331, Met332, Val333, Phe538, Leu659, Asn660, Lys661, Trp695, Ser749, Ser760, Tyr761, and Glu801. These residues help with the exact positioning of the isoalloxazine moiety and the substrate that is required for catalysis. Among them, Arg310, Arg316, Lys661, Tyr761, and Glu801 may have different protonation states depending on the pH of the environment; the same applies to four residues on the H3 tail (H3R2, H3K4, H3K9, and H3K14). Since the active site of LSD1 is shielded against solvent access, substrate binding is expected to lead to changes in the acidity/basicity of the active-site residues. To check for possible changes in the protonation states of these residues upon substrate binding, we computed their acid dissociation constant (pK_a) values at the optimum-activity pH = 8.7 of LSD1[9] (Table 1) using H++ webserver.[53] Judging from the pK_a values in the absence of protein, the methylation site H3K4 (sLys, pK_a = 10.4) should be protonated (as well as the other lysines and arginine located on the H3 tail). Upon binding of the H3 tail to LSD1, H3K4 becomes more acidic (with the pK_a value changing from 10.4 to 6.5), suggesting that it will lose a proton to the microenvironment, while the other residues on the tail remain protonated. This is in line with the need of a

Table 1. Computed Acid Dissociation Constants (pK_a Values) of Selected Residues in Model Systems Containing Only the H3 Tail, Only LSD1, or Both of Them in a Complex, in the Absence and Presence of FAD and Crystal Water (at pH = 8.7)[a]

	without FAD			with FAD	
residue ID	only H3	only LSD1	LSD1 + H3	only LSD1	LSD1 + H3
R2	>12.0	–	>12.0	–	>12.0
H3K4 (sLys)	10.4	–	<0	–	6.5
H3K9	10.6	–	>12.0	–	11.1
H3K14	9.2	–	>12.0	–	>12.0
R310	–	>12.0	>12.0	>12.0	>12.0
R316	–	8.2	7.7	9.3	7.6
K661	–	11.2	7.5	7.4	3.4
Y761	–	>12.0	>12.0	>12.0	>12.0
E801	–	<0	<0	<0	<0

[a]Values in the left (right) panel were obtained without (with) FAD and crystal water molecules being included in the analysis (to show their effect on the pK_a values of the active-site residues).

dx.doi.org/10.1021/ja403582u | J. Am. Chem. Soc. 2013, 135, 13400–13413

deprotonated (neutral) amine site for proper oxidation, as has also been observed for other amine oxidases.[9,20]

The active-site residues surrounding the isoalloxazine moiety may act as a base and accept a proton from sLys. To identify a suitable active-site base, we calculated the pK_a values of these residues (Table 1). R316, K661, and E801 are predicted to have low pK_a values, but K661 is the only residue that is properly placed near the substrate and can be involved in proton transfer. The significant decrease in pK_a value upon binding of FAD and sLys to LSD1 suggests that the conserved K661 residue will lose a proton to bulk water via the microenvironment and can thereafter accept a proton from sLys. Although the exact mechanism for such a proton loss is not known, a breathing motion of the protein may assist this process, as has been proposed previously for another amine oxidase, DAAO.[54]

The residue Tyr761, which is part of the aromatic cage conserved in most amine oxidases and is in close proximity to sLys, was also considered as a potential active-site base. However, as evident from Table 1, Tyr 761 remains protonated after FAD and substrate binding, thus preventing the uptake of a proton. This supports the steric role of the conserved tyrosine residue for proper orientation of sLys (rather than a function as active-site base).

Protonation State of Substrate Lysine (sLys) and K661: MD Simulation Results. In order to gain deeper insight into the binding of the sLys in the active site, we performed a series of 20 ns MD simulations. We generated four different NVT ensembles by considering two different protonation states of K661 and sLys, which will be referred to as follows: (a) protonated sLys, sLys-NMe_2H^+; (b) deprotonated sLys, sLys-NMe_2; (c) protonated K661, K661-NH_3^+; and (d) deprotonated K661, K661-NH_2. In addition, the effect of mutating K661 into a methionine (K661M) was also investigated in two additional NVT ensembles (one for sLys-NMe_2H^+ and another one for sLys-NMe_2).

In the simulation of the protein with both lysines protonated (sLys-NMe_2H^+ and Lys661-NH_3^+), sLys remains far separated from the reactive center of flavin (i.e., the distance between FAD and sLys is more than 6 Å): sLys-NMe_2H^+ thus fails to bind, presumably because of the electrostatic repulsion in the active site. This underscores the necessity of Lys661 being deprotonated (neutral) for effective substrate binding. In the remaining five NVT ensembles with other protonation state combinations and with K661M, sLys is found to be located properly, close to and above the *re*-face of the isoalloxazine moiety of FAD, as required for amine oxidation. This positioning has also been observed for other amine oxidases.[17] There are two distinct binding modes of sLys at the reaction center (N5 of FAD) in these ensembles, depending on the chosen protonation state of sLys. These two orientations are termed "upward" and "downward" according to the alignment of the other (i.e. non-reacting) methyl group of sLys with respect to the C4a–N5 bond of FAD. They are depicted in Figure 3, along with our labeling convention for the atoms.

In the MD simulation with sLys-NMe_2H^+ and Lys661-NH_2, the protonated sLys prefers the downward orientation. It is linked to a water bridge consisting of three water molecules connected through H-bonds with the help of W695 (Figure 4). This three-water-bridge motif is an extension of the Lys–H_2O–N5 motif conserved in most amine oxidases, by incorporation of two additional water molecules. The water bridge is crucial since it connects sLys to FAD and K661, and thus provides a route for the proton shuttle from sLys to K661 in accord with

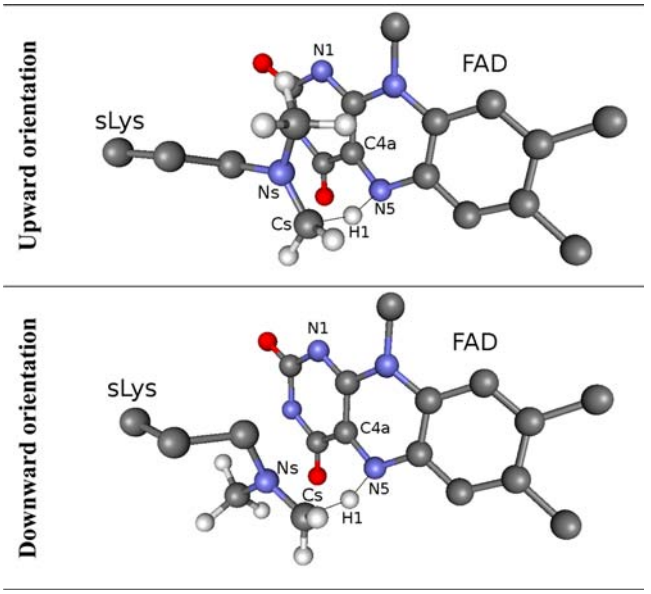

Figure 3. Ball-and-stick representations of the upward (top panel) and downward (bottom panel) orientations of sLys. The notation reflects the orientation of the non-reacting methyl group of sLys with respect to the N5–C4a bond of FAD. The structures show parts of the QM region from the QM/MM optimized **1-TS** geometries, with most of the hydrogen atoms, the deprotonated K661, and the three QM water molecules removed for clarity. Also included is the numbering of the relevant atoms (used in the text). The standard flavin numbering scheme has been adopted along with special atom labels for the substrate lysine (Cs and Ns). H1 is the hydride equivalent being transferred.

the theoretical pK_a analysis. The stability of the water bridge is supported by the solvent-inaccessible design of the active site of LSD1, which is common to all amine oxidases.[17] W695 is located at the catalytic center (see Figure 4) and remains part of the water bridge during the entire MD simulation (see Supporting Information, Figure S1). It affords extra stabilization by hydrogen-bonding, and along with Y761 it controls the traffic of water molecules in the active site. The loss of LSD1 activity upon W695A mutation[25] can therefore be related to the resulting disruption of the water bridge. These findings support an important structural role for W695 in amine oxidation.

In the MD simulation with K661M and sLys-NMe_2H^+, we do not observe formation of the three-water-bridge motif in the K661M mutant. In this case, there is no residue that could serve as an H-bond donor/acceptor residue and connect to the isoalloxazine moiety of flavin via the conserved water molecule. Moreover, the methyl group of methionine in K661M will not lose a proton upon substrate binding and will thus not act as active-site base. The profound loss of enzymatic activity of LSD1 upon K661A mutation[18] can be ascribed to the lack of an effective proton shuttle from sLys to K661. This further supports the active-site base role of the conserved K661.

An already deprotonated sLys prefers to bind in upward orientation in the active site. In this orientation, the electrostatic interaction between two partially charged atoms (Ns of sLys and C4a of FAD) and the orbital interaction of the lone pair of sLys-Ns with the π^*-orbital (C4a–N5) of FAD help keeping the reactive partners for amine oxidation in the two subunits (N5 in FAD and Cs in sLys) in close contact. Selected average distances and angles derived from the NVT ensembles with Lys661-NH_3^+, Lys661-NH_2, and K661M are

dx.doi.org/10.1021/ja403582u | J. Am. Chem. Soc. 2013, 135, 13400–13413

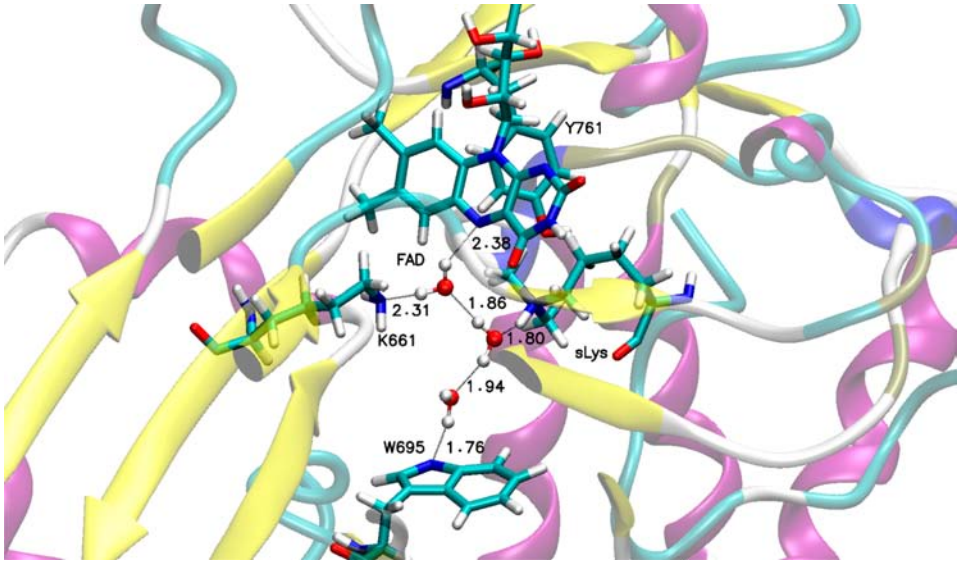

Figure 4. Typical snapshot showing the three-water-bridge motif in the downward orientation. Hydrogen bonds are marked with thin black lines; the corresponding distances are given in Å. The snapshot was taken from an MD simulation with sLys-NMe_2H^+ and Lys661-NH_2 (see text).

Table 2. Average Distances (Å) and Angles (degree) (with the Corresponding Standard Deviations) for Three Different NVT Ensembles with Deprotonated Substrate K4 (sLys)

structural property	deprotonated K661	protonated K661	K661M mutant
R(Ns−C4a)	3.23 ± 0.13	3.26 ± 0.14	3.14 ± 0.12
R(N5−Cs)	3.78 ± 0.26	3.84 ± 0.25	3.64 ± 0.23
θ(Cs−Ns−C4a−N5)	−34.0 ± 7.1	−16.8 ± 6.9	−32.4 ± 8.0
R(N5−H (H_2O))[a]	2.10 ± 0.34	1.98 ± 0.21	N/A

[a]H(H_2O) is the hydrogen of the conserved crystal water hydrogen-bonded to N5 of FAD.

compiled in Table 2. In all three cases, proper binding of sLys on top of the FAD plane is achieved, and the two subunits stay in close contact during the MD simulations. This suggests that the binding mode of deprotonated sLys with respect to FAD is affected significantly neither by the protonation state nor even by the mutation of K661. Therefore, if sLys has already lost its extra proton prior to binding in the active site (which is unlikely, given the usual pH of the environment), the protonation state of K661 is of no concern for proper binding of sLys.

These findings are in accordance with experimentally observed circular dichroism spectra and structural studies,[19] which indicate that K300M mutation in mPAO does not affect substrate binding and overall protein folding, even though the reaction rate is slowed down about 1400-fold. In contrast, the K661−H_2O−N5 motif cannot be formed in the K661M mutant (independent of the protonation state of sLys), whereas it is formed in wild-type LSD1 for both protonation states of K661, with a slight variation in the distance of this conserved lysine to the conserved water molecule (Table 2). Thus, our MD simulation results highlight the role of the K661 residue as an active-site base and the importance of the water bridge for mediating the proton shuttle between sLys and K661.

QM-Only and QM/MM Results. We carried out QM-only and QM/MM calculations to locate the stationary points of the two main proposed catalytic mechanisms (HT and SET, Figure 1). As starting geometries for QM/MM calculations, we used five different snapshots for each orientation, which were chosen randomly from two different MD simulation trajectories (i.e., Lys661-NH_2 with sLys-NMe_2H^+ for upward orientation and Lys661-NH_2 with sLys-NMe_2H^+ for downward orientation). The QM-only studies were performed on a model system consisting of sLys, the isoalloxazine ring of FAD, and two active-site water molecules. In a preliminary conformational analysis at the B3LYP level, we found that the components of the model system are completely free to move (and relax) due to the absence of constraints from the protein environment. As a consequence, the two distinct QM-only TSs for the HT pathway with downward and upward orientation differ by less than 0.5 kcal/mol in energy; for the sake of brevity, we limited our analysis at the QM-only level to the downward HT pathway. In the case of the SET mechanism, the QM-only optimizations yielded only one single TS (regardless of the chosen starting geometry). The gas-phase QM-only energetics obtained with four different DFT functionals are compiled in Table 3 and visualized in Figure S2. B3LYP yields activation barriers for the HT and SET mechanisms that are somewhat lower than those predicted by the other functionals (by 1−2, 1−8, and 2−5 kcal/mol compared to M06-2X, LC-ωPBE, and mPW1K, respectively). More importantly, however, the relative Gibbs free energies of the different stationary points exhibit the same trends for all four functionals. To limit the computational effort, we have therefore decided to apply only B3LYP in the further calculations.

Considering the crucial role of K661 and the three-water-bridge motif in the MD simulations (*vide supra*), the QM/MM calculations were performed with a standard QM region composed of sLys (side chain), the isoalloxazine moiety of FAD, K661, and the three bridging water molecules (72−73 QM atoms). Two different orientations of sLys (upward and

Table 3. QM-Only Relative Gibbs Free Energies (kcal/mol) for the Stationary Points (As Given in Figure 1) Evaluated Using Different DFT Functionals and the 6-31G* Basis Set[a]

	B3LYP-gas	B3LYP-water	M06-2X	LC-ωPBE	mPW1K
Direct Hydride Transfer (HT; Singlet Manifold)					
^{1}**RC**	0.0	0.0	0.0	0.0	0.0
^{1}**TS**	31.0	26.7	33.0	32.2	36.4
^{1}**PC**	15.5	12.4	7.2	9.4	4.5
Radical Mechanism (SET; Triplet Manifold)					
^{3}**RC**	35.1	30.2	35.6	42.5	37.5
^{3}**TS**	37.9	36.5	38.4	46.2	39.9
^{3}**PC**	29.8	26.9	27.7	36.4	25.5

[a]The present B3LYP/6-31G* results are in good agreement with those reported previously.[33]

downward, see Figure 3) were considered for modeling the stationary points of the two proposed reductive half-reaction mechanisms (HT and SET). Keeping in mind the importance of the protonation state of K661 for the binding of sLys in the active site (*vide supra*), the stationary points were modeled using different protonation states of K661, namely K661-NH_2 and K661-NH_3^+. In contrast, only deprotonated sLys was considered in the QM/MM calculations. The QM/MM relative energies and free energies for all possible combinations are compiled in Table 4 and visualized in Figure 5. All these values are computed as the average over five different sets of QM/MM calculations starting from five different snapshots taken randomly along the course of the corresponding NVT ensemble (see Supporting Information, Tables S1 and S2). Table 4 also contains the QM/MM energetics for the K661M mutant (as visualized in Figure S3), obtained as the average of two sets of calculations (see Table S3).

To check the effect of basis set extension, we also provide single-point QM(B3LYP-D/TZVPP)/MM relative energies computed at QM(B3LYP-D/6-31G*)/MM geometries (see Table S4). Similarly, we check the effect of expanding the standard QM region by including the residues Gly330, Met332, Val333, Thr335, Tyr761, and Val811, which form an extensive H-bond network to FAD and sLys (see Figure S4, upper panel). For this extended QM region (with 173−174 QM atoms depending on the protonation state of K661), we performed single-point QM(B3LYP-D/6-31G*)/MM energy calculations at the available optimized QM/MM geometries. The resulting energetics is given in Table S5. Evidently, the use of the larger basis set and of the extended QM region lowers the relative energies by ca. 2−3 kcal/mol, but the trends remain the same. Therefore, we shall focus in the following on the results of QM(B3LYP-D/6-31G*)/MM calculations with the standard QM region.

In the model systems with protonated K661, the TSs always have higher Gibbs free energies (relative to ^{1}**RC**) than their counterparts with deprotonated K661 (Table 4). For the sake of brevity, we will only discuss the results for the latter case when comparing the different pathways in upward and downward orientation. The effects of K661 protonation and K661M mutation will be addressed in a later section.

Hydride Transfer (HT) Mechanism. The HT mechanism involves the transfer of a proton and two electrons from sLys to FAD in a single concerted step (as H^- anion). It is generally considered as the most likely route for the rate-determining C−H bond oxidation step of LSD1-catalyzed lysine demethylation. A closed-shell description at the RKS level is well suited for this process that converts the reactant complex ^{1}**RC** via the transition state ^{1}**TS** to the product complex ^{1}**PC**. Hybrid QM/MM calculations predict free energy barriers of 20.9 ± 1.1 and 15.4 ± 1.0 kcal/mol for the HT mechanism with upward and downward orientation of sLys, respectively (Table 4). By contrast, QM-only calculations yield barriers of 31.0 kcal/mol in vacuum and 26.7 kcal/mol in water. The HT rate is thus increased dramatically by the protein environment.

Key structural properties for the stationary points are compiled in Tables 5 and 6 at the QM-only and QM/MM levels, respectively. Evidently, ^{1}**RC**, ^{1}**TS** and ^{1}**PC** are predicted to be more compact in the enzyme, both for the upward and downward orientation, i.e., the two reacting subunits (sLys and FAD) stay closer to each other in the protein environment. This effect of the environment is most pronounced for ^{1}**TS**. The corresponding optimized geometries are visualized in Figure 3 (QM/MM) and Figure S5 (QM). The QM/MM structures of ^{1}**TS** are quite similar for the upward and downward orientation, but rather different from the QM optimized structures. In the QM/MM TSs, the lysine tail is oriented parallel to the C4a−N5 π-bond in an optimum distance for the HT to the acceptor orbital. The optimized distances for the breaking Cs− H1 bond are 1.39 and 1.37 Å, whereas those for the forming N5−H1 bond are 1.24 and 1.25 Å, for the upward and downward orientation, respectively (Table 6), implying a late TS for HT pathway. The HT angle (N5−H1−Cs) is almost identical in both orientations (ca. 154°). The QM-only calculations also yield a late TS with the same HT angle (154°), but the bond distances for Cs−H1 (1.50 Å) and N5−H1 (1.16 Å) deviate appreciably. The Wiberg

Table 4. QM(B3LYP-D/6-31G*)/MM Relative Energies (Gibbs Free Energies in Parentheses) for the Stationary Points (see Figure 1) in Upward and Downward Orientation and for the K661M Mutant: Average Values and Standard Deviations (kcal/mol) over a Set of Five Snapshots

	deprotonated K661		protonated K661		
	upward	downward	upward	downward	K661M
Direct Hydride Transfer (HT; Singlet Manifold)					
^{1}**RC**	0.00 (0.00)	0.00 (0.00)	0.00 (0.00)	0.00 (0.00)	0.00 (0.00)
^{1}**TS**	23.8 ± 1.93 (20.9 ± 1.14)	18.9 ± 0.95 (15.4 ± 0.98)	25.1 ± 2.05 (21.7 ± 2.12)	23.5 ± 2.97 (20.0 ± 2.75)	22.4 ± 1.0 (19.0 ± 1.1)
^{1}**PC**	2.05 ± 0.95 (2.42 ± 0.94)	−12.5 ± 3.57 (−12.1 ± 3.53)	13.5 ± 1.54 (13.7 ± 1.50)	15.8 ± 1.49 (15.6 ± 1.38)	1.80 ± 1.6 (1.60 ± 2.5)
Radical Mechanism (SET; Triplet Manifold)					
^{3}**RC**	31.5 ± 2.28 (31.1 ± 2.28)	20.9 ± 1.89 (20.4 ± 1.70)	29.5 ± 2.63 (29.2 ± 2.66)	24.6 ± 1.85 (24.2 ± 1.82)	27.2 ± 0.5 (26.9 ± 0.5)
^{3}**TS**	48.0 ± 1.71 (44.2 ± 1.72)	37.1 ± 1.76 (33.2 ± 1.73)	49.3 ± 2.78 (45.6 ± 2.81)	44.7 ± 3.22 (41.1 ± 2.99)	48.2 ± 0.6 (44.4 ± 0.7)
^{3}**PC**	27.9 ± 1.38 (27.4 ± 1.37)	24.5 ± 2.27 (23.8 ± 2.36)	35.3 ± 2.88 (35.2 ± 2.85)	37.9 ± 3.14 (37.2 ± 3.37)	32.2 ± 0.6 (31.9 ± 0.7)

dx.doi.org/10.1021/ja403582u | J. Am. Chem. Soc. 2013, 135, 13400−13413

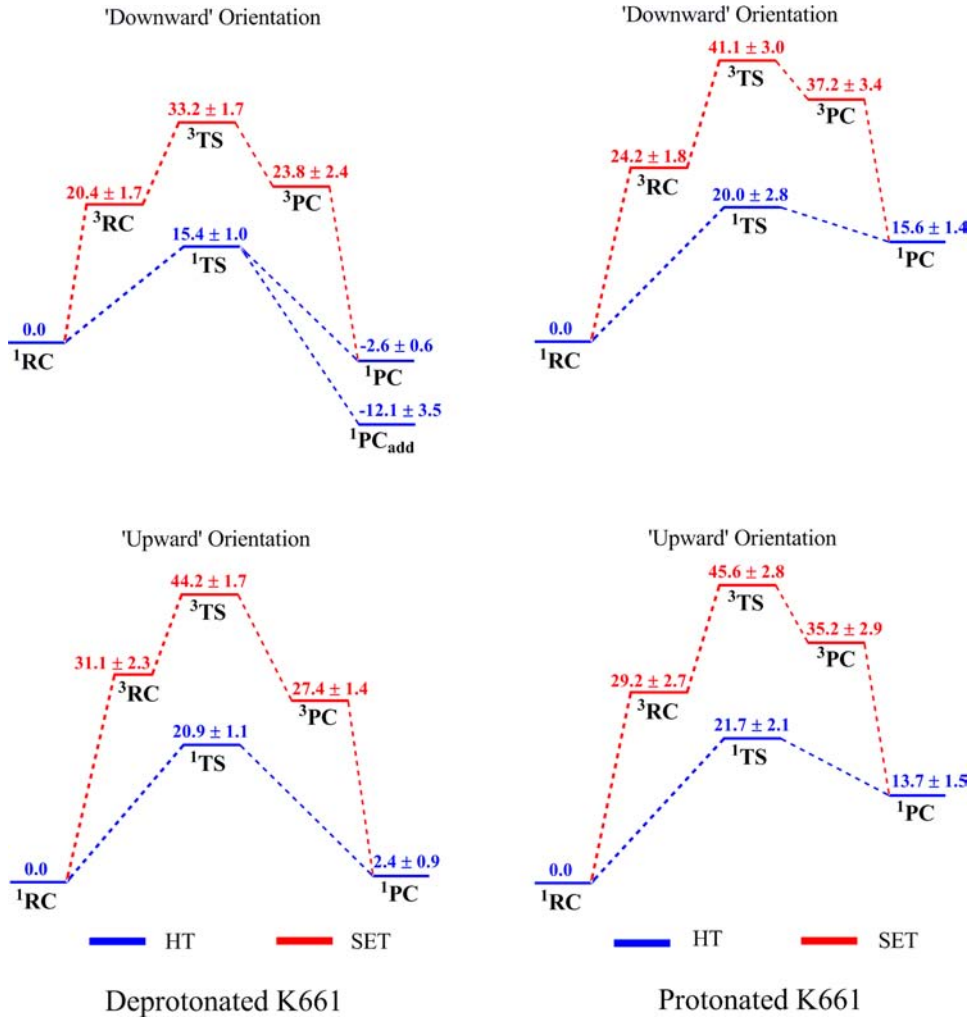

Figure 5. QM(B3LYP-D/6-31G*)/MM Gibbs free energy profiles (in kcal/mol) for HT and SET pathways obtained with deprotonated (left) and protonated (right) K661 and with downward and upward orientation. See Figure 1 for the definition of the stationary points. The profiles were computed with deprotonated sLys. The upper-left diagram includes the free energies both of the weakly interacting product complex ^{1}**PC** and the adduct ^{1}**PC**$_{add}$ (see text for details).

Table 5. Selected Distances (*R*, in Å), Angles, and Dihedral Angles (θ, in Degree) from QM-Only Optimizations of the Stationary Points at the B3LYP-D/6-31G* Level

	^{1}RC	^{1}TS	^{1}PC	^{3}RC	^{3}TS	^{3}PC
θ(Cs−H1−N5)	111.3	153.6	48.0	158.2	167.6	92.7
R(N5−H1)	3.00	1.16	1.05	2.96	1.37	1.04
R(Cs−H1)	1.10	1.50	2.21	1.10	1.35	3.38
R(Ns−C4a)	3.15	2.96	3.06	3.97	4.10	4.52
R(Cs−N5)	3.55	2.60	1.70	3.34	2.71	3.58
R(Cs−Ns)	1.46	1.35	1.37	1.45	1.39	1.46
R(C4a−N5)	1.30	1.38	1.46	1.37	1.37	1.37
θ(Ns−Cs−N5−C4a)	30.2	−0.6	46.7	−44.2	4.9	48.7

bond order ratio (Cs−H1 vs N5−H1) is around 0.85 in all ^{1}**TS** geometries (see Table S6).

As the HT reaction proceeds, the developing charges on the Ns$^{\delta-}$ (sLys) and C4a$^{\delta+}$ (FAD) atoms will provide some electrostatic stabilization, since the interacting centers C4a and Ns become sufficiently close at the TS (QM-only, 2.96 Å; QM/MM upward, 2.81 Å; QM/MM downward, 2.79 Å, indicating a stronger effect in the enzyme). Orbital interactions between the lone pair on sLys-Ns and the π*-orbital (C4a−N5) of FAD may be important both in the reactant complex ^{1}**RC** and the transition state ^{1}**TS**. The HOMOs at the ^{1}**RC** and ^{1}**TS** geometries in both upward and downward orientation are shown in Figure 6. In the case of ^{1}**RC** (Figure 6, upper panel) with upward orientation, the lone pair at Ns of sLys is aligned such that it lies almost orthogonal to the plane of π-conjugation on the isoalloxazine ring of FAD. This stacked orientation of cofactor and substrate enhances the overlap between the orbitals of the two subunits that can stabilize this ^{1}**RC** species. By contrast, in downward orientation, ^{1}**RC** adopts a nonstacked alignment between the two reacting subunits that offers little

dx.doi.org/10.1021/ja403582u | J. Am. Chem. Soc. 2013, 135, 13400−13413

Table 6. Selected Distances (R, in Å), Angles, and Dihedral Angles (θ, in Degree) of Stationary Points with Upward and Downward Orientation (Deprotonated K661) Obtained from QM(B3LYP-D/6-31G*)/MM Optimizations

	upward orientation						downward orientation					
	^{1}RC	^{1}TS	^{1}PC[a]	^{3}RC	^{3}TS	^{3}PC	^{1}RC	^{1}TS	^{1}PC[a]	^{3}RC	^{3}TS	^{3}PC
θ(Cs−H1−N5)	112.4	154.6	54.6	98.9	152.8	81.2	99.9	153.6	48.1	120.7	155.4	102.6
R(N5−H1)	2.59	1.24	1.03	2.72	1.22	1.06	2.66	1.25	1.07	2.56	1.31	1.07
R(Cs−H1)	1.10	1.39	2.62	1.09	1.50	3.64	1.09	1.37	2.17	1.12	1.39	3.97
R(Ns−C4a)	2.69	2.81	2.94	2.84	3.11	3.08	2.74	2.79	2.92	3.16	3.20	3.64
R(Cs−N5)	3.18	2.57	2.19	3.08	2.64	3.63	3.04	2.55	1.66	3.28	2.64	4.33
R(Cs−Ns)	1.46	1.36	1.31	1.45	1.38	1.38	1.46	1.36	1.38	1.44	1.38	1.38
R(C4a−N5)	1.30	1.37	1.42	1.37	1.37	1.36	1.30	1.37	1.45	1.37	1.37	1.37
θ(Ns−Cs−N5−C4a)	−25.3	−21.7	−24.0	−26.4	−31.8	−34.5	10.2	3.9	46.2	−1.2	−14.3	−6.7

[a]The column ^{1}PC contains the structural parameters of the weakly interacting product complex for upward orientation, and those of the adduct for downward orientation.

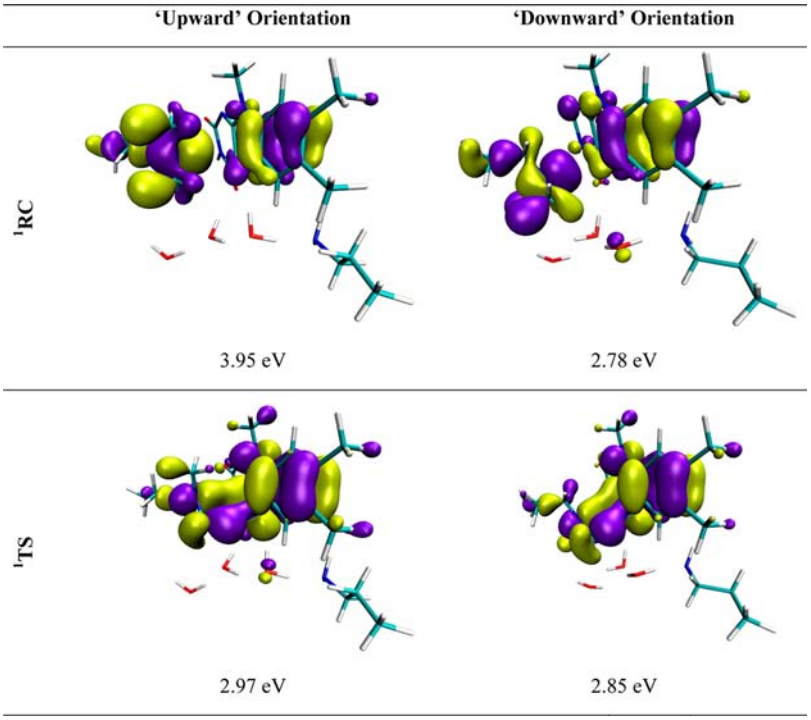

Figure 6. Highest occupied molecular orbital (HOMO) isosurfaces of ^{1}RC and ^{1}TS in upward and downward orientation. HOMO−LUMO gaps are given in eV. A contour value of 0.02 was chosen for creating the isosurfaces using VMD.

stabilization. On the other hand, in the ^{1}TS structures both for upward and downward orientation, the two reacting units assume a proper stacking orientation that allows enhanced orbital interactions. These findings may rationalize the lower activation barrier for the HT mechanism in downward orientation where ^{1}RC is less stabilized compared to upward orientation. To estimate the intrinsic magnitude of the associated energetic effect, TSs with different lysine orientations, which lack the C4a···Ns interaction, were modeled and optimized at the QM-only level: they were found to have higher energies (by 3−6 kcal/mol) than the reference QM-only TS.

The Cs···N5 interaction becomes crucial in the product complex ^{1}PC as the lone pair is now located on N5 rather than Ns. The Cs−N5 distance is computed to be 1.66 and 2.19 Å in downward and upward orientation, respectively. In the former case, a FAD-sLys adduct complex is formed, which is not possible in the latter case due to steric congestion. Consequently, ^{1}PC is significantly more stable in downward than in upward orientation, as can be seen from the reaction free energies (−12.1 ± 3.5 vs 2.4 ± 0.9 kcal/mol). Although the adduct formation in ^{1}PC in downward orientation is predicted to be a barrierless process that will occur readily, we tried to find the weakly interacting PC (with Cs−N5 distance of more than 2 Å), for direct comparison with the upward case. In two out of the five snapshots, by rearranging the water-bridge motif, we could locate a weakly interacting ^{1}PC minimum, with a reaction free energy of −2.63 kcal/mol (average value). Hence, the HT in downward orientation remains mildly exergonic even in this case (and does not become endergonic as in upward orientation). To study the interconversion of the two minima, we performed a one-dimensional relaxed potential energy scan for one of the snapshots using the Cs−N5 distance as the reaction coordinate. The resulting energy profile indicates facile formation of the adduct from the weakly interacting complex, with a barrier of less than 1 kcal/mol (see Figure S9).

Radical Single-Electron Transfer (SET) Mechanism. The radical SET mechanism involves intermediates (Figure 1). It starts with the activation of the αC−H bond of lysine by an

dx.doi.org/10.1021/ja403582u | J. Am. Chem. Soc. 2013, 135, 13400−13413

initial SET to the flavin to yield two monoradical intermediates (^{3}**RC**), namely the amine radical cation (**sLys**$^{\bullet+}$) and flavin semiquinone anion (**FAD**$^{\bullet-}$ or **Fl**$^{\bullet-}$). The subsequent rate-limiting step is the homolytic cleavage of the αC−H bond that generates the iminium cation (^{1}**PC**). It may proceed via two different paths. One is proton-coupled electron transfer (PCET), which is also called the direct hydrogen atom transfer path, whereas the other one involves consecutive transfers of a proton and an electron (second SET) from the amine to the flavin. In the latter case, the proton transfer leads to an intermediate pair of ammonium and **FADH**$^{\bullet-}$ radicals (^{3}**PC**), and the second SET step can occur directly or may also be mediated by adduct formation in the presence of an active-site radical.[28] To properly describe the open-shell species on the SET pathways, we employed the UKS treatment. As the two unpaired electrons on two different subunits of the model system can have the same or different spin, both the singlet and triplet manifolds were considered. In the case of the singlets, the UKS calculations as well as restricted open-shell Kohn−Sham (ROKS) calculations always converged to the closed-shell solutions as can be seen from the resulting energies (see Table S7) and spin densities (data not shown). Therefore, we only present the triplet UKS results for the SET mechanism; the stationary points are named accordingly, i.e., ^{3}**RC**, ^{3}**TS**, and ^{3}**PC**.

The first SET from **sLys** to **FAD**, yielding ^{3}**RC**, is predicted to be energetically demanding. QM-only calculations (without protein environment) give high barriers in the gas phase and in water (35.1 and 30.2 kcal/mol, respectively). We could not precisely determine the energy needed for intersystem crossing ($S_0 \rightarrow T_1$), which is however expected to be lower than that of the transition state ^{3}**TS** for the subsequent proton transfer from **sLys**$^{\bullet+}$ to **FAD**$^{\bullet-}$.[9] Indeed, the overall activation barrier for homolytic cleavage of the αC−H bond is 37.9 and 36.5 kcal/mol in the gas phase and in water, respectively; the energy lowering by the water environment is thus less than in the case of HT pathway (1.4 vs 4.3 kcal/mol). The generated radicals (^{3}**PC**) are also rather unstable, with energies of 29.8 and 26.9 kcal/mol, respectively, relative to ^{1}**RC**. The QM/MM calculations generally predict somewhat lower relative energies for ^{3}**RC**, ^{3}**TS**, and ^{3}**PC**, but the trends in the energetics are the same (Table 4). The protein environment is computed to lower the activation barrier of the SET pathway by ca. 5 kcal/mol when sLys is aligned in the downward orientation, but this barrier is still about twice as high as that for the HT pathway. In downward orientation, ^{3}**TS**, ^{3}**RC**, and ^{3}**PC** are all stabilized relative to ^{1}**RC**, which reflects the already discussed destabilization of ^{1}**RC** (see above). In upward orientation, the relative energies of these species are generally higher. Once the first SET is realized and the ^{3}**RC** species is formed, the subsequent proton transfer from **sLys**$^{\bullet+}$ to **FAD**$^{\bullet-}$ is predicted to have a relatively low barrier (with respect to ^{3}**RC**), both at the QM-only level and at the QM/MM level (see Tables 3 and 4). These low barriers are kinetically irrelevant, because the SET mechanism is inaccessible due to the high initial barrier for the formation of ^{3}**RC**.

Key structural features of the optimized stationary points from the QM-only and QM/MM calculations are presented in Tables 5 and 6, respectively. As for the HT pathway, the reactive core of the stationary points on the SET pathway is generally more compact in the protein environment. However, contrary to the HT case, the downward orientation leads to a significantly looser binding of the two subunits in all species (see R(Ns−C4a) in ^{3}**RC**, ^{3}**TS**, and ^{3}**PC**), which should alleviate any unfavorable interactions among the unpaired electron density distributed over the two subunits and may thus help to stabilize the downward orientation. In line with the latter, the products of the SET mechanism (^{3}**PC**) do not form an adduct complex, as opposed to the products of the HT mechanism (^{1}**PC**). In the transition state ^{3}**TS**, the proton-transfer angle θ(Cs−H1−N5) is 153−155° in both upward and downward orientation, and thus the same as in the HT case (^{1}**TS**), see Table 6. In the QM-only gas-phase calculations, this angle is significantly larger in ^{3}**TS** (168°, Table 5), presumably since sLys may move in the absence of protein constraints toward a more linear arrangement utilizing another acceptor orbital (i.e., the lone pair at N5). The protein environment enforces a transfer angle of 153−155° and the involvement of a singly occupied π acceptor orbital. This difference in the TS geometries is reflected in the proton transfer barriers of the QM-only (2.8 kcal/mol) and QM/MM calculations (13.1 and 12.8 kcal/mol in upward and downward orientation, respectively).

The spin densities computed for ^{3}**RC**, ^{3}**TS**, and ^{3}**PC** with upward and downward orientation of sLys are given in Figure S6. Evidently, the stationary points on the SET pathway generally contain sLys and FAD radicals as shown in Figure 1; in downward orientation, one of the conserved water molecules may also accommodate some unpaired electron density.

Effects of K661 and Y761 on the Reaction. In this section, we discuss the effects of the active-site residues on the LSD1-mediated amine oxidation reaction. Homologues of the active-site LSD1 residues K661 and Y761 are highly conserved among the members of the amine oxidase family and are expected to play a crucial role in the reactions catalyzed by amine oxidases. As noted in the MD simulations, K661 supports the formation of the three-water-bridge motif and the downward orientation with less stable reactants (sLys and FAD). Besides, theoretical pK_a analysis suggests that K661 may get deprotonated upon binding of sLys in the active site. To further augment our understanding of the effect of K661 protonation on the catalysis, we performed QM/MM calculations with K661 in its protonated form for both the downward and upward orientation of sLys. The resulting QM/MM energies are presented in Table 4. Compared with the case of deprotonated K661, protonated K661 yields the same trends in the energetics, but the activation barriers are higher (by 1−6 kcal/mol) for the HT and SET pathways in each orientation. Notably, the downward orientation of sLys yields lower barriers than the upward orientation for both pathways. The most dramatic change in the energetics is predicted for ^{1}**PC** and ^{3}**PC**, which are both destabilized with respect to the corresponding ^{1}**RC** species.

To identify possible causes of this destabilization of the PC species, some key structural properties of the stationary points from the QM/MM calculations with protonated K661 are compiled in Table S8. As can be seen from the Cs−N5 distances (3.14 and 2.98 Å), there is no adduct formation in ^{1}**PC** (not even in downward orientation) when K661 is protonated. Comparison of ^{1}**PC** geometries in downward orientation with deprotonated and protonated K661 (see Figure 7) reveals different H-bonding networks for the different protonation states. In ^{1}**PC** with protonated K661, the three involved water molecules are arranged such that they form an H-bond to N5 of FAD at one end and accept an H-bond from protonated K661 at the other end. As a consequence, the lone

dx.doi.org/10.1021/ja403582u | J. Am. Chem. Soc. 2013, 135, 13400−13413

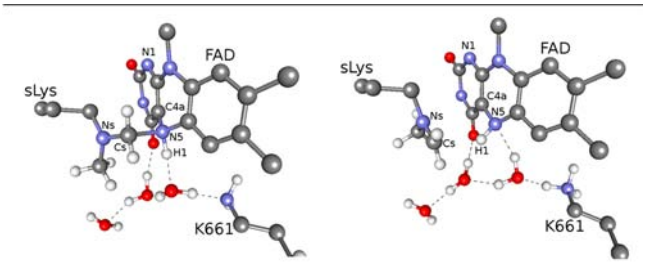

Figure 7. Comparison of product complexes ^{1}**PC** when K661 is deprotonated (left) and protonated (right). Adduct formation following hydride transfer depends on the protonation state of K661. H-bonds are indicated by black dashed lines. Some hydrogens are not shown for clarity.

electron pair on N5 is not freely available for adduct formation. These findings confirm that the deprotonated form of K661 is required for adduct formation between sLys and FAD, which is, in turn, needed to make the overall process exothermic.

Despite the fact that K661 plays a crucial role in the demethylation process by supporting H-bonding networks and acting as an active-site base, it is not expected to have a catalytic role in LSD1,[9] in contrast to the MPAO case.[19] To check the validity of this notion, we performed MD simulations for each of the two protonation states of sLys with K661 being mutated into methionine. As already discussed above, these runs for the K661M mutant do not show any binding of protonated sLys (Cs−N5 distance larger than 6 Å). On the other hand, in the unlikely event that sLys is already deprotonated initially, the MD run indicates that it may bind properly in front of *re*-face of FAD in a reactive distance with an upward-type orientation (Table 2). To analyze the effects of K661M mutation on the HT and SET energy profiles, we performed corresponding QM/MM calculations. Comparing the structural properties of the optimized stationary points for the wild-type enzyme in upward orientation and for the K661M mutant (see Tables 6 and S9) we generally find high similarity in the computed geometries, with particularly remarkable agreement in the case of ^{1}**TS** and ^{3}**TS**. Likewise, the calculated relative energies for the wild-type enzyme (upward orientation) and the mutant are in almost perfect agreement, within 1 kcal/mol, both for the HT and SET pathway (see Table 4). In addition, the QM/MM calculations (see Figure S6) do not give any unpaired electron density on the K661/M661 unit in any case (regardless of protonation state or sLys orientation), thus suggesting no role for this residue in electron transfers on the SET pathway. Taken together, these findings strongly support the notion that the catalytic mechanism of LSD1 is not dependent on the K661 residue. Therefore, the complete loss of LSD1 activity upon K661 mutation[18] can be ascribed to its role as active-site base that accepts a proton from protonated sLys prior to substrate binding.

In the MD runs with each of the six NVT ensembles, the other conserved residue, Y761, was found to stay in close contact with sLys (data not shown), in line with its anticipated role of orienting sLys in front of the flavin. In addition to this steric role, Y761 has also been considered as the active-site base and as the initial single electron acceptor in the radical mechanism.[1,23] We exclude both these possibilities as follows. To check the suitability of Y761 as active-site base, we performed a series of QM/MM calculations to compare the energy change upon proton transfer from sLys to Y761 and K661 (the only candidates for an active-site base). The proton transfer to deprotonated K661 is computed to be downhill by 9 kcal/mol. On the contrary, a minimum with protonated Y761 ($Y\text{-}OH_2^+$) could not be found as all optimization efforts ended up with back-transfer of the proton to sLys. If we assume Y761 to be deprotonated initially ($Y\text{-}O^-$) the proton transfer from sLys is calculated to be exothermic by 5−6 kcal/mol. However, this is a highly unrealistic assumption, for the following reasons: (a) theoretical pK_a analysis predicts Y761 to be neutral (Y-OH) after sLys binding; (b) no base stronger than tyrosine is present in the binding pocket to generate the tyrosyl anion; and (c) Y761F mutation does not lead to complete loss of LSD1 activity as in the case of K661A mutation.[25] Considering the possibility that Y761 might act as initial single electron acceptor in LSD1, we computed the QM/MM spin densities (see Figure S4) using an extended QM region that included Y761 and several neighboring residues. We find that neither Y761 nor any other of these residues can accommodate unpaired electron density, thus ruling out a role as single-electron acceptor that would stabilize the reactant species (^{3}**RC**) on the SET pathway.

■ DISCUSSION

C−H bond activation represents an elementary step of many enzymatic reactions and is often achieved by the use of metal-containing active sites capable of activating the inert C−H bond. By contrast, LSD1 catalyzes amine (αC−H bond) oxidation in a metal-free manner. Studies on various amine oxidases[17] have shown that the oxidative power of flavin can be significantly enhanced by the flavoprotein environment, making it potent enough to oxidize the C−H bond of a methyl group. Several mechanisms have been proposed in the literature for the rate-determining C−H bond cleavage step during amine oxidation, namely HT, SET, and adduct-forming mechanisms (involving carbanions and polar nucleophiles). The goal of this work is to clarify the mechanism of LSD1-catalyzed amine oxidation through MD simulations as well as QM-only and QM/MM calculations. Toward this goal, we also investigated the role of active-site LSD1 residues, namely K661, Y761, and W695.

The present computational results provide detailed insight into the mechanism of the reductive half-reaction (i.e., amine oxidation). Energetically (see Tables 3 and 4), the HT mechanism is clearly favored over the SET mechanism, for which the overall activation barrier is about twice as high. For the SET mechanism, we could not identify Tyr761 or any other active-site residue as candidate (instead of FAD) for accepting the initial electron from sLys in our QM/MM calculations. Therefore, the high energy required to form initial radicals (^{3}**RC**) and the resulting high overall barrier for the SET pathway are not diminished by the involvement of neighboring protein residues. This is not the case for MAO-A, which has been reported to form a tyrosyl radical that is in equilibrium with a flavosemiquinone radical: This tyrosyl-flavin radical pair is long-lived enough to be visible in EPR and ENDOR spectra.[23,24] The main reason for the absence of such a stable radical formation in the case of LSD1 is probably the non-covalent binding of FAD to LSD1, as opposed to the covalent binding in the case of MAO-A.

The present theoretical calculations introduce two distinct orientations (upward and downward) of the non-reacting methyl group of sLys with respect to the C4a−N5 bond of FAD. Our calculations predict an amenable barrier for C−H bond oxidation (via the HT pathway) for each of the two

dx.doi.org/10.1021/ja403582u | J. Am. Chem. Soc. 2013, 135, 13400−13413

orientations, as opposed to the rather high barrier of 32 kcal/mol reported previously.[39] The computations also show that the flavoprotein environment can keep sLys in the less stable downward orientation, which in turn reduces the activation barrier for the HT mechanism by about 5 kcal/mol. The computed activation barrier in upward orientation (20.9 kcal/mol) corresponds to a rate of 0.17 min^{-1}, which is in seemingly good agreement with the experimentally observed average turnover rate of LSD1 with the substrate dimethyl lysine (8.10 ± 0.20 min^{-1}).[8] The less stable downward orientation (with a barrier of 15.4 kcal/mol) leads to a much higher reaction rate of 1330 min^{-1}; this overestimate of the rate is consistent with the well-known tendency of B3LYP to underestimate barrier heights.[46,55] The water-bridge motif and the protein environment are found to be vital for supporting this less stable orientation.

The QM/MM-level ^{15}N KIEs with Wigner tunneling corrections do not provide any clear preference for the HT or SET mechanism in LSD1, like in the case of MTOX[33] (see Table S10 for results, computational details, and comparison to the MTOX results). The ^{15}N KIE values are reverse (less than unity) and in good agreement with the computed and observed values for MTOX.[33] They are insensitive to different sLys orientations, unlike the deuterium KIE values for sLys with trideuterated methyl groups, which are found to be more sensitive (see Table S10). Compared with the downward orientation, the computed deuterium KIE values for the upward orientation are smaller (for both mechanisms) and closer to experiment (4.0 ± 0.2). However, as tunneling effects for hydrogen are quite pronounced and cannot be fully accounted by the Wigner corrections, we refrain from conclusions based on such comparisons with experiment.

The MD simulations with different protonation states of K661 and sLys indicate that the protonation state of K661 is crucial for binding sLys in the active site. If K661 and sLys are both kept protonated in an NVT ensemble, sLys does not properly bind, presumably because of electrostatic repulsions; it binds only when either sLys or K661 or both are deprotonated. To accommodate sLys in the active site in its protonated form (sLys-NH_3^+), protonated K661 (K661-NH_3^+) needs to release its proton to the microenvironment in order to accept the extra proton from sLys. This initial proton transfer prior to the demethylation process is crucial, since it ensures the availability of the lone pair on the amine moiety of sLys for the oxidation step. It is computed to be quite facile, with a QM/MM activation barrier of 8.4 kcal/mol for the proton transfer from sLys-NH_3^+ to K661-NH_2. The proton shuttle between sLys and K661 is supported by an extended water-bridge motif that involves three active-site water molecules and deprotonated K661. In all MD simulations, the three water molecules remain in the space between sLys, FAD, and K661; the W695 tryptophan residue fortifies the water-bridge motif through hydrogen-bonding (Figure 4), which is essential as seen from the significant loss of LSD1 activity observed upon W695 mutation.[25] In the case of the K661M mutant, the absence of the water-bridge motif prevents an efficient proton transfer, which is probably the main reason for the experimentally observed complete loss of LSD1 activity.[18] The computed QM/MM energy profiles show that K661M mutation has almost no effect on the activation barriers of the HT and the SET mechanism. It thus appears that K661 has no catalytic role in LSD1, as opposed to its analogue (K300) in maize polyamine oxidase (MPAO).[19] Instead, K661 is likely to act as the active site-base that initially accepts a proton from sLys. Although the protonation state of K661 does not significantly affect the rates of the HT pathway, the QM/MM energy profiles indicate that it controls the stability of the product species (^{1}**PC**): protonated K661 prevents formation of the iminium-FADH adduct and leads to an endothermic process, whereas deprotonated K661 allows for such adduct formation in an exothermic process (in downward orientation). This again underscores the need for having deprotonated K661 in the active site before and after substrate binding.

The other conserved active-site residue, Y761, stays in close proximity to sLys during the MD simulations. It helps to align the substrate in front of the *re*-face of the isoalloxazine ring of FAD via steric (repulsive) interactions. Our current calculations suggest that Y761 does not act as an active-site base or an initial electron acceptor, which has sometimes been assumed to be its role as a member of the aromatic cage motif conserved in amine oxidases.[23] Therefore, given its mere steric role, Y761 would not seem indispensable for the amine oxidation process, which is line with the only partial reduction of LSD1 activity upon Y761F mutation.[25]

As an alternative to the HT and SET pathways, adduct-forming mechanisms have been proposed in the literature.[29] They involve concerted or nonconcerted heterolytic cleavage of the αC−H bond and nucleophilic attack of the lone pairs on the amino nitrogen atom of the substrate. Depending on the type of proton acceptor, there are two types of adduct-forming mechanisms. In the carbanion mechanism, an active-site residue abstracts a proton from the αC−H bond of sLys (Cs−H1), whereas in the polar nucleophilic mechanism the N5 atom of FAD makes a nucleophilic attack on the proton (H1); the C4a atom of FAD is the electrophilic center and prone to the nucleophilic attack from the Ns atom of sLys. Methyl C−H activation is a demanding process that requires a very strong base. In LSD1, K661 is the only available active-site base present in the crystal structure,[10] which is able to extract the extra proton from the amine site (Ns) of sLys, but it is not potent enough to activate the C−H bond. Therefore, the carbanion mechanism can be ruled out for LSD1. Likewise, although the polar nucleophilic mechanism is considered feasible for the amine oxidation mediated by MAO-A and MAO-B,[29,56] it is quite unlikely for LSD1 due to the bulkiness of the substrate (caused by the methyl groups bonded to Ns of sLys), which will destabilize any adduct species located on Ns because of unfavorable steric interactions with the flavin rings. Our QM/MM calculations indicate that such adduct species (by covalent bonding of Ns of sLys with C4a of FAD) are less stable than the species appearing along the HT pathway (by covalent bonding of Cs of sLys with N5 of FAD).

We also investigated the feasibility of some other conceivable pathways for amine oxidation. First, we tried to transfer a hydride equivalent from the αC−H bond of sLys to the N1 instead of the N5 position, both via HT and SET mechanisms. This reaction has to surmount significantly higher activation barriers in both cases (60.5 and 48.8 kcal/mol for HT and SET, respectively), presumably due to the steric shielding of the N1 position by nearby LSD1 residues (Thr810 and Val811). These residues are likely to stabilize the reduced flavin ($FADH^-$) formed via HT, as has been suggested for other flavoenzymes.[17] Moreover, the HT pathway was previously predicted to have a lower barrier in the gas phase if the N1 atom were protonated prior to the transfer.[33] However, our QM/MM calculations predict a very high barrier of ca. 90 kcal/mol for the

dx.doi.org/10.1021/ja403582u | J. Am. Chem. Soc. 2013, 135, 13400−13413

protonation of the N1 position, demonstrating that this process is not feasible in the protein environment.

CONCLUSION

Classical MD simulations as well as QM-only and QM/MM calculations were performed to elucidate the catalytic mechanism of the rate-determining amine oxidation step in LSD1-mediated demethylation of histone tail lysine. We find that the hydride transfer (HT) pathway is clearly favored over other proposed mechanisms, including the radical (or single-electron transfer, SET) route as well as the carbanion and polar-nucleophilic mechanisms. QM/MM calculations predict activation barriers in the range of 15−21 kcal/mol for the α-CH bond cleavage on the HT pathway, in reasonable agreement with the experimentally observed rates.

The various features of LSD1 that facilitate oxidative CH bond cleavage were analyzed in detail. It was shown that substrate lysine can assume two distinct orientations in the binding pocket relative to the isoalloxazine moiety of FAD, which are denoted as downward and upward based on the orientation of the non-reacting methyl group of sLys. The computed activation barriers for the HT and SET pathways with downward orientation of sLys are consistently lower than those with the alternative upward orientation. In both orientations, the lone pair on sLys lies almost orthogonal to the FAD-isoalloxazine ring, allowing for favorable n(sLys)−π*-(C4a−N5 of FAD) orbital interactions at the rate-limiting HT TS. This TS is further stabilized by electrostatic interactions with the surrounding protein environment, as can be seen from the barriers computed with (15−21 kcal/mol) and without (31 kcal/mol) the protein environment. The QM/MM calculations also provide an explanation why the SET pathway is disfavored in LSD1. In the SET mechanism, the first electron transfer from sLys to FAD generates a sLys-FAD radical pair (^{3}**RC**), which is much higher in energy than the closed-shell reactant complex (^{1}**RC**). This is mainly due to the inability of surrounding LSD1 residues (in particular Y761) to delocalize the unpaired electron density in the ^{3}**RC** species and to form a stable radical pair with FAD (replacing sLys as partner of FAD).

Several active-site LSD1 residues (K661, Y761, and W695) and the conserved water-bridge motif assist the catalysis in a number of ways: Y761 has only a steric effect in positioning the reaction partners properly; K661 acts as an active-site base; and the water bridge is crucial for promoting the proton transfer, with W695 shielding and stabilizing this bridge (in line with experimental point mutation studies). According to our calculations, K661 plays a crucial role in the LSD1-mediated demethylation of lysine substrates: K661 will get deprotonated as sLys (mostly present in the protonated form, sLys-NH_3^+) enters the binding pocket and will then act as the base to accept a proton from sLys, thus helping to "liberate" the Ns(sLys) lone pair that is required for the subsequent transfer of a hydride equivalent to FAD; moreover, deprotonated K661 is required to make the overall HT process exothermic by allowing adduct formation in the product species (^{1}**PC**). The studies on the K661M mutant provide further information: the computed barriers for the HT and SET pathways are essentially unaffected by the mutation, indicating that K661 does not have a direct catalytic influence in amine (sLys) oxidation. On the contrary, the active-site base role of K661 is supported by MD simulations showing that K661M mutation disrupts the water-bridge motif and thus prevents deprotonation of sLys-NH_3^+ after binding to LSD1; this will reduce LSD1 activity (as also confirmed experimentally).

To summarize, our results on LSD1 are consistent with the available experimental evidence and the basic results of a recent computational investigation.[39] The present study goes beyond previous work by providing comprehensive insight into the LSD1-mediated dimethylamine (lysine) oxidation at the molecular level, which may be helpful for designing novel inhibitor molecules suitable for controlling an abnormal demethylation/methylation balance.

ASSOCIATED CONTENT

Supporting Information

Detailed information on model system preparation, optimized geometries of various stationary points, various structural properties, QM/MM energies, energy profiles, Wiberg bond orders, spin densities, ^{2}H and ^{15}N KIEs, and visualization of the extended QM region and of frontier orbitals. This material is available free of charge via the Internet at http://pubs.acs.org.

AUTHOR INFORMATION

Corresponding Author

thiel@kofo.mpg.de

Present Address

[†]M.P.: Centre for Excellence in Basic Sciences, Health Centre, University of Mumbai, Vidhyanagari Campus, Mumbai 400098, India

Notes

The authors declare no competing financial interest.

ACKNOWLEDGMENTS

B.K. acknowledges Profs. Burak Erman and Ozlem Keskin for valuable discussions at an early stage of this study.

REFERENCES

(1) Forneris, F.; Battaglioli, E.; Mattevi, A.; Binda, C. *FEBS J.* **2009**, *276*, 4304−4312.
(2) Hu, P.; Zhang, Y. *J. Am. Chem. Soc.* **2006**, *128*, 1272−1278.
(3) Culhane, J. C.; Cole, P. A. *Curr. Opin. Chem. Biol.* **2007**, *11*, 561−568.
(4) Shi, Y.; Whetstine, J. R. *Mol. Cell* **2007**, *25*, 1−14.
(5) Yang, M.; Culhane, J. C.; Szewczuk, L. M.; Jalili, P.; Ball, H. L.; Machius, M.; Cole, P. A.; Yu, H. *Biochemistry* **2007**, *46*, 8058−8065.
(6) Paik, W.; Kim, S. *Biochem. Biophys. Res. Commun.* **1973**, *51*, 781−788.
(7) Shi, Y.-J.; Lan, F.; Matson, C.; Mulligan, P.; Whetstine, J.; Cole, P.; Casero, R. A.; Shi, Y. *Cell* **2004**, *119*, 941−953.
(8) Forneris, F.; Binda, C.; Dall'Aglio, A.; Fraaije, M. W.; Battaglioli, E.; Mattevi, A. *J. Biol. Chem.* **2006**, *281*, 35289−35295.
(9) Gaweska, H.; Henderson Pozzi, M.; Schmidt, D. M. Z.; McCafferty, D. G.; Fitzpatrick, P. F. *Biochemistry* **2009**, *48*, 5440−5445.
(10) Forneris, F.; Binda, C.; Adamo, A.; Battaglioli, E.; Mattevi, A. *J. Biol. Chem.* **2007**, *282*, 20070−20074.
(11) Chen, Y.; Yang, Y.; Wang, F.; Wan, K.; Yamane, K.; Zhang, Y.; Lei, M. *Proc. Natl. Acad. Sci. U.S.A.* **2006**, *103*, 13956−13961.
(12) Huang, J.; Sengupta, R.; Espejo, A. A. B.; Lee, M. M. G.; Dorsey, J. a J.; Richter, M.; Opravil, S.; Shiekhattar, R.; Bedford, M. T.; Jenuwein, T.; Berger, S. L. *Nature* **2007**, *449*, 105−109.
(13) Wang, J.; Hevi, S.; Kurash, J. K.; Lei, H.; Gay, F.; Bajko, J.; Su, H.; Sun, W.; Chang, H.; Xu, G.; Gaudet, F.; Li, E.; Chen, T. *Nat. Genet.* **2009**, *41*, 125−129.
(14) Cho, H.-S.; Suzuki, T.; Dohmae, N.; Hayami, S.; Unoki, M.; Yoshimatsu, M.; Toyokawa, G.; Takawa, M.; Chen, T.; Kurash, J. K.;

Field, H. I.; Ponder, B. a J.; Nakamura, Y.; Hamamoto, R. *Cancer Res.* **2011**, *71*, 655−660.
(15) Smith, B. C.; Denu, J. M. *Biochim. Biophys. Acta* **2009**, *1789*, 45−57.
(16) Lohse, B.; Kristensen, J. L.; Kristensen, L. H.; Agger, K.; Helin, K.; Gajhede, M.; Clausen, R. P. *Bioorg. Med. Chem.* **2011**, *19*, 3625−3636.
(17) Fraaije, M. W.; Mattevi, A. *Trends Biochem. Sci.* **2000**, *25*, 126−132.
(18) Lee, M. G.; Wynder, C.; Cooch, N.; Shiekhattar, R. *Nature* **2005**, *437*, 432−435.
(19) (a) Polticelli, F.; Basran, J.; Faso, C.; Cona, A.; Minervini, G.; Angelini, R.; Federico, R.; Scrutton, N. S.; Tavladoraki, P. *Biochemistry* **2005**, *44*, 16108−16120. (b) Fiorillo, A.; Federico, R.; Polticelli, F.; Boffi, A.; Mazzei, F.; Di Fusco, M.; Ilari, A.; Tavladoraki, P. *FEBS J.* **2011**, *278*, 809−821.
(20) Pozzi, M. H.; Gawandi, V.; Fitzpatrick, P. F. *Biochemistry* **2009**, *48*, 1508−1516.
(21) Pozzi, M. H. *Arch. Biochem. Biophys.* **2010**, *498*, 83−88.
(22) Bruckner, R. C.; Winans, J.; Jorns, M. S. *Biochemistry* **2011**, *50*, 4949−4962.
(23) Li, M.; Binda, C.; Mattevi, A.; Edmondson, D. E. *Biochemistry* **2006**, *45*, 4775−4784.
(24) Rigby, S. E. J.; Hynson, R. M. G.; Ramsay, R. R.; Munro, A. W.; Scrutton, N. S. *J. Biol. Chem.* **2005**, *280*, 4627−4631.
(25) Stavropoulos, P.; Blobel, G.; Hoelz, A. *Nat. Struct. Mol. Biol.* **2006**, *13*, 626−632.
(26) Silverman, R. B.; Hoffman, S. J.; Catus, W. B. *J. Am. Chem. Soc.* **1980**, *102*, 7126−7128.
(27) Silverman, R. B. *Acc. Chem. Res.* **1995**, *28*, 335−342.
(28) Silverman, R. B. *Prog. Brain Res.* **1995**, *106*, 23−31.
(29) Miller, J. R.; Edmondson, D. E. *Biochemistry* **1999**, *38*, 13670−13683.
(30) Gaweska, H.; Fitzpatrick, P. F. *BioMol. Concepts* **2011**, *2*, 365−377.
(31) Scrutton, N. S. *Nat. Prod. Rep.* **2004**, *21*, 722−730.
(32) Fitzpatrick, P. F. *Arch. Biochem. Biophys.* **2010**, *493*, 13−25.
(33) Ralph, E. C.; Hirschi, J. S.; Anderson, M. A; Cleland, W. W.; Singleton, D. A; Fitzpatrick, P. F. *Biochemistry* **2007**, *46*, 7655−7664.
(34) Schmidt, D. M. Z.; McCafferty, D. G. *Biochemistry* **2007**, *46*, 4408−4416.
(35) McCann, A. E.; Sampson, N. S. *J. Am. Chem. Soc.* **2000**, *122*, 35−39.
(36) Chen, Z.; Zhao, G.; Martinovic, S. *Biochemistry* **2005**, 15444−15450.
(37) Forneris, F.; Binda, C.; Vanoni, M. A.; Mattevi, A.; Battaglioli, E. *FEBS Lett.* **2005**, *579*, 2203−2207.
(38) Karasulu, B.; Keskin, O.; Erman, B. In *5th International Symposium on Health Informatics and Bioinformatics*; IEEE: Antalya, 2010; pp 197−205.
(39) Kong, X.; Ouyang, S.; Liang, Z.; Lu, J.; Chen, L.; Shen, B.; Li, D.; Zheng, M.; Li, K. K.; Luo, C.; Jiang, H. *PLoS One* **2011**, *6*, e25444.
(40) Brooks, B. R.; Brooks, C. L., III; MacKerell, A. D.; Nilsson, L.; Petrella, R. J.; Roux, B.; Won, Y.; Archontis, G.; Bartels, C.; Boresch, S.; Caflisch, A.; Caves, L.; Cui, Q.; Dinner, A. R.; Feig, M.; Fischer, S.; Gao, J.; Hodoscek, M.; Im, W.; Kuczera, K.; Lazaridis, T.; Ma, J.; Ovchinnikov, V.; Paci, E.; Pastor, R. W.; Post, C. B.; Pu, J. Z.; Schaefer, M.; Tidor, B.; Venable, R. M.; Woodcock, H. L.; Wu, X.; Yang, W.; York, D. M.; Karplus, M. *J. Comput. Chem.* **2009**, *30*, 1545−1615.
(41) Ryckaert, J.-P.; Ciccotti, G.; Berendsen, H. J. *J. Comput. Phys.* **1977**, *23*, 327−341.
(42) Frisch, M. J.; Trucks, G. W.; Schlegel, H. B.; Scuseria, G. E.; Robb, M. A.; Cheeseman, J. R.; Scalmani, G.; Barone, V.; Mennucci, B.; Petersson, G. A.; Nakatsuji, H.; Caricato, M.; Li, X.; Hratchian, H. P.; Izmaylov, A. F.; Bloino, J.; Zheng, G.; Sonnenberg, J. L.; Hada, M.; Ehara, M.; Toyota, K.; Fukuda, R.; Hasegawa, J.; Ishida, M.; Nakajima, T.; Honda, Y.; Kitao, O.; Nakai, H.; Vreven, T.; Jr., J. A. M.; Peralta, J. E.; Ogliaro, F.; Bearpark, M.; Heyd, J. J.; Brothers, E.; Kudin, K. N.; Staroverov, V. N.; Kobayashi, R.; Normand, J.; Raghavachari, K.; Rendell, A.; Burant, J. C.; Iyengar, S. S.; Tomasi, J.; Cossi, M.; Rega, N.; Millam, J. M.; Klene, M.; Knox, J. E.; Cross, J. B.; Bakken, V.; Adamo, C.; Jaramillo, J.; Gomperts, R.; Stratmann, R. E.; Yazyev, O.; Austin, A. J.; Cammi, R.; Pomelli, C.; Ochterski, J. W.; Martin, R. L.; Morokuma, K.; Zakrzewski, V. G.; Voth, G. A.; Salvador, P.; Dannenberg, J. J.; Dapprich, S.; Daniels, A. D.; Farkas, O.; Foresman, J. B.; Ortiz, J. V.; Cioslowski, J.; Fox, D. J. *Gaussian 09*, Revision A.02; Gaussian Inc.: Pittsburgh, PA, 2009.
(43) Becke. *J. Chem. Phys.* **1993**, *98*, 5648−5652.
(44) Zhao, Y.; Truhlar, D. G. *Theor. Chem. Acc.* **2007**, *120*, 215−241.
(45) Vydrov, O. A; Scuseria, G. E. *J. Chem. Phys.* **2006**, *125*, 234109.
(46) Lynch, B. J.; Fast, P. L.; Harris, M.; Truhlar, D. G. *J. Phys. Chem. A* **2000**, *104*, 4811−4815.
(47) Sherwood, P.; de Vries, A. H.; Guest, M. F.; Schreckenbach, G.; Catlow, C. R. A.; French, S. A.; Sokol, A. A.; Bromley, S. T.; Thiel, W.; Turner, A. J.; Billeter, S.; Terstegen, F.; Thiel, S.; Kendrick, J.; Rogers, S. C.; Casci, J.; Watson, M.; King, F.; Karlsen, E.; Sjovoll, M.; Fahmi, A.; Schäfer, A.; Lennartz, C. *J. Mol. Struct. THEOCHEM* **2003**, *632*, 1−28.
(48) Ahlrichs, R.; Bär, M.; Baron, H. -P.; Bauernschmitt, S.; Böcker, S.; Ehrig, M.; Eichkorn, K.; Elliott, S.; Furche, F.; Haase, F.; Häser, M.; Horn, H.; Huber, C.; Huniar, U.; Kattannek, M.; Kölmel, C.; Kollwitz, M.; May, K.; Ochsenfeld, C.; Öhm, H.; Schäfer, A.; Schneider, U.; Treutler, O.; von Arnim, M.; Weigend, F.; Weis, P.; Weiss, H. *TURBOMOLE*, v. 6.3; 2011.
(49) Grimme, S. *J. Comput. Chem.* **2006**, *27*, 1787−1799.
(50) Smith, W.; Forester, T. R. *J. Mol. Graphics* **1996**, *14*, 136−141.
(51) de Vries, A. H.; Sherwood, P.; Collins, S. J.; Rigby, A. M.; Rigutto, M.; Kramer, G. J. *J. Phys. Chem. B* **1999**, *103*, 6133−6141.
(52) Billeter, S. R.; Turner, A. J.; Thiel, W. *Phys. Chem. Chem. Phys.* **2000**, *2*, 2177−2186.
(53) Gordon, J. C.; Myers, J. B.; Folta, T.; Shoja, V.; Heath, L. S.; Onufriev, A. *Nucleic Acids Res.* **2005**, *33*, W368−371.
(54) Harris, C.; Pollegioni, L.; Ghisla, S. *Eur. J. Biochem.* **2001**, *268*, 5504−5520.
(55) Lingwood, M.; Hammond, J. R.; Hrovat, D. A.; Mayer, J. M.; Borden, W. T. *J. Chem. Theory Comput.* **2006**, *2*, 740−745.
(56) Edmondson, D. E.; Binda, C.; Mattevi, A. *Arch. Biochem. Biophys.* **2007**, *464*, 269−276.